

# Electronic structure and magnetism of disordered bcc Fe alloys

Subhradip Ghosh, Biplab Sanyal<sup>†</sup>, Chhanda Basu Chaudhuri  
and Abhijit Mookerjee

S.N.Bose National Centre for Basic Sciences, JD Block, Sector 3, Salt Lake City,  
Calcutta 700091, India

<sup>†</sup> Department of Physics, Brock University, St. Catharines, Ontario L2S 3A1, Canada.

**Abstract.** We here study electronic structure and magnetic properties of disordered bcc  $\text{Co}_x\text{Fe}_{1-x}$ ,  $\text{Cr}_x\text{Fe}_{1-x}$  and  $\text{Mn}_x\text{Fe}_{1-x}$  alloys in their ferromagnetic phases using Augmented Space Recursion (ASR) technique coupled with tight-binding linearized muffin tin orbital (TB-LMTO) method. We calculate the densities of states, magnetic moments and Curie temperatures of these alloys to show the variation upon alloying Fe with the other neighbouring 3-*d* transition metals using arguments based on charge transfer, exchange splitting and hybridization effects.

## 1. Introduction

Properties of magnetic materials have been a subject of great scientific and practical interest. An enormous amount of experimental and theoretical investigations has been carried out to have a proper understanding of the nature of magnetism in solids [1]. Fe, being one of the ferromagnets among the late transition metals has drawn considerable attention due to its interesting magnetic properties. Apart from studies on elemental Fe which include the studies on structural [2] and magnetic phase stability [3, 4, 5] there are numerous investigations on magnetism in Fe based ordered and disordered alloys, both theoretically and experimentally. The experimental investigations have provided a variety of information about the magnetic properties of these systems e.g. variation of magnetization with band filling [6, 7], moment distribution in dilute Fe alloys in low [8]

as well as in finite temperatures [9], local environmental effects on magnetic properties [10, 11], spatial distribution and thermal variation of hyperfine fields [12], concentration dependence of high field susceptibility [13], low temperature specific heat [14, 15] and magnetic phase stability leading eventually to magnetic phase diagrams [16].

The earlier theoretical studies were based on various models of band structure calculations [17, 18]. Though these calculations were successful to a certain extent in explaining the experimental observations, they suffered from the drawback of having too many adjustable parameters which limited the reliability of their results. But, with the recent progresses in first principles electronic structure techniques, the properties of magnetic alloys are investigated more accurately and efficiently. Different aspects of magnetism in both ordered and disordered phases of Fe alloys have been studied successfully by these techniques overcoming the limitations of earlier model calculations [19, 20, 21, 22]. In this communication, we aim at a systematic study of electronic structure and magnetic properties of substitutionally disordered  $\text{Co}_x\text{Fe}_{1-x}$ ,  $\text{Cr}_x\text{Fe}_{1-x}$  and  $\text{Mn}_x\text{Fe}_{1-x}$  alloys using the self-consistent TBLMTO-ASR technique. In the elemental phase, bcc Fe is a ferromagnet, bcc Cr is a weak non-commensurate antiferromagnet, Mn has a very complicated crystal (unit cell of 58 atoms) and magnetic structure while Co is a ferromagnet. For FeCr, Fe atoms stabilize the commensurate antiferromagnetic (B2) order in the Cr-rich side ( $x > 0.8$ ) although  $\text{Cr}_x\text{Fe}_{1-x}$  with  $x > 0.8$  are ferromagnets and stabilize in bcc lattice [23]. In case of MnFe alloys, ferromagnetic phase is stable only up to  $x = 0.2$  and the crystal stabilizes in bcc lattice. For  $x > 0.2$ , several phases with antiferromagnetic ordering get stabilized [24]. In FeCo alloys, however, the ferromagnetic phase is stable for the full range of concentrations and the crystal too stabilizes in the bcc structure. To our knowledge, no systematic study on these three systems has been done so far using the same methodology, though they are four

successive members on the same row of periodic table. This motivated us to perform a systematic investigation of these systems. In this work, we have restricted ourselves only to the ferromagnetic phases of these systems.

## 2. Theoretical Details

To study these alloys we will use the methodology of the augmented space recursion technique [25, 26, 27] in the first principles framework of tight-binding linearized muffin tin orbital method [28]. Extensive details of the description of the effective augmented-space Hamiltonian have been given in an earlier paper[29]. Here we shall quote the key results of generalized TBLMTO-ASR .

$$\begin{aligned}
H &= \sum_{RL} \hat{C}_{RL} \mathcal{P}_{RL} + \sum_{RL} \sum_{R'L'} \hat{\Delta}_{RL}^{1/2} S_{RL,R'L'}^{\beta} \hat{\Delta}_{R'L'}^{1/2} \mathcal{T}_{RL,R'L'} \\
\hat{C}_{RL} &= C_{RL}^B + (C_{RL}^A - C_{RL}^B) n_R \\
\hat{\Delta}_{RL}^{1/2} &= \Delta_{RL}^{B1/2} + (\Delta_{RL}^{A1/2} - \Delta_{RL}^{B1/2}) n_R
\end{aligned} \tag{1}$$

Here  $\mathcal{P}_{RL}$  and  $\mathcal{T}_{RL,R'L'}$  are projection and transfer operators in the Hilbert space spanned by the tight binding basis  $|RL\rangle$  and  $n_R$  is a random occupation variable which is 1 if the site  $R$  is occupied by an atom of the A type and 0 if not.  $C_{RL}^Q$  and  $\Delta_{RL}^Q$  are potential parameters describing the scattering properties of the constituents(Q=A, B) of the alloy and  $S_{RL,R'L'}^{\beta}$  is the screened structure constant describing the geometry of the underlying lattice. The augmented space Hamiltonian replaces the random occupation variable by operators  $M_R$  of rank 2. For models without any short-range order

$$\begin{aligned}
M_R &= x \mathcal{P}_{\uparrow}^R + (1-x) \mathcal{P}_{\downarrow}^R + \sqrt{x(1-x)} (\mathcal{T}_{\uparrow\downarrow}^R + \mathcal{T}_{\downarrow\uparrow}^R) \\
|\uparrow\rangle &= (\sqrt{x}|0\rangle + \sqrt{1-x}|1\rangle)
\end{aligned}$$

$$|\downarrow\rangle = (\sqrt{1-x}|0\rangle - \sqrt{x}|1\rangle)$$

The recursion method then expresses the Green functions as continued fraction expansions. The continued fraction coefficients are exactly obtained up to eight levels and the terminator suggested by Luchini and Nex [30] is used to approximate the asymptotic part. The convergence of this procedure has been discussed by Ghosh *et al* [31]. The local charge densities are given by :

$$\rho_\sigma^\lambda(r) = (-1/\pi)\Im m \sum_L \int_{-\infty}^{E_F} dE \ll G_{LL}^{\lambda,\sigma}(r, r, E) \gg \quad (2)$$

Here  $\lambda$  is either  $A$  or  $B$ . The local magnetic moment is

$$m^\lambda = \int_{r < R_{WS}} d^3r [\rho_\uparrow(r) - \rho_\downarrow(r)]$$

The Curie temperature  $T_C$  can be calculated using Mohn-Wolfarth model [32] from the expression

$$\frac{T_C^2}{T_C^S} + \frac{T_C}{T_{SF}} - 1 = 0$$

where,  $T_c^S$  is the Stoner Curie temperature calculated from the relation

$$\langle I(E_F) \rangle \int_{-\infty}^{\infty} N(E) \left( \frac{\delta f}{\delta E} \right) dE = 1 \quad (3)$$

$\langle I(E_F) \rangle$  is the concentration averaged Stoner parameter. The parameters of pure elements are obtained from the earlier calculations [33],  $N(E)$  is the density of states per atom per spin [34] and  $f$  is the Fermi distribution function.  $T_{SF}$  is the spin fluctuation temperature given by,

$$T_{SF} = \frac{m^2}{10k_B \langle \chi_0 \rangle} \quad (4)$$

$\langle \chi_0 \rangle$  is the concentration weighted exchange enhanced spin susceptibility at equilibrium and  $m$  is the averaged magnetic moment per atom.  $\chi_0$  (pure elements) is calculated

using the relation by Mohn [32] and Gersdorf [35]:

$$\chi_0^{-1} = \frac{1}{2\mu_B^2} \left( \frac{1}{2N^\uparrow(E_F)} + \frac{1}{2N^\downarrow(E_F)} - I \right)$$

$I$  is the Stoner parameter for pure elements and  $N^\uparrow(E_F)$  and  $N^\downarrow(E_F)$  are the spin-up and spin-down partial density of states per atom at the Fermi level for each species in the alloy.

### 3. Computational Details

For our calculations we have used a real space cluster of 400 atoms and an augmented space shell up to the sixth nearest neighbour from the starting state. Eight pairs of recursion coefficients were determined exactly and the continued fraction terminated by the analytic terminator due to Luchini and Nex [30]. In a paper Ghosh *et al* [31] have shown the convergence of the related integrated quantities, like the Fermi energy, the band energy, the magnetic moments and the charge densities, within the augmented space recursion. The convergence tests suggested by the authors were carried out to prescribed accuracies. We noted that at least eight pairs of recursion coefficients were necessary to provide Fermi energies and magnetic moments to required accuracies. We have reduced the computational burden of the energy dependent recursion method using the seed recursion methodology [37] with fifteen energy seed points uniformly across the spectrum.

We have varied the Wigner-Seitz radii of the two constituent atoms in order to have charge neutral spheres. This eliminates the necessity to calculate the Madelung energy which is a difficult task for the case of disordered alloys. Simultaneously we have made sure that the sphere overlap remains within the 15% limit prescribed by Andersen.

The calculations have been made self-consistent in the LSDA sense, that is, at each stage

the averaged charge densities are calculated from the augmented space recursion and the new potential is generated by the usual LSDA techniques. This self-consistency cycle was converged in both total energy and charge to errors of the order  $10^{-5}$ . The exchange-correlation potential of Von Barth and Hedin has been used,  $s, p$  and  $d$  orbitals were used to construct the basis functions and scalar relativistic corrections were included. For all the calculations, we have used the lattice constants for the alloys according to Vegard's law.

#### 4. Results and Discussion

In our approach we emphasize on interrelations of magnetism and charge transfer behaviour. Since in our calculations we have maintained local charge neutrality, we have to deal with the question of strong variation of magnetic moments. Within the itinerant electron theory of magnetism this can be understood in terms of a redistribution of local electronic charge either between two spin directions. Together with Coulomb interaction which determines the positions of atomic  $d$  levels of the constituents and thus the charge transfer in case of a transition metal alloy, magnetic exchange and hybridization play very important role in determining the magnetic properties. This has already been observed in certain cases [39, 40].

These facts can be expressed in a more quantitative form using  $d$ -orbital potential parameters  $C_{d\sigma}^Q$  obtained from TBLMTO for both alloy components ( $Q=A, B$ ) and for both spin directions ( $\sigma=\uparrow, \downarrow$ ). These quantities are equivalent to the atomic  $d$  levels. The spin dependent diagonal disorder in a random binary alloy  $A_xB_{1-x}$  can be defined as [38] ,

$$\delta_\sigma = C_{d\sigma}^A - C_{d\sigma}^B \tag{5}$$

The local exchange splitting can be defined as [38],

$$\Delta_e^Q = C_{d\downarrow}^Q - C_{d\uparrow}^Q \quad (6)$$

Figure 1 shows the compositional dependence of local and average magnetic moments for  $\text{Co}_x\text{Fe}_{1-x}$  alloys. The filled triangles denote the average moments while the filled circles denote Fe moment and filled squares denote Co moments. The open triangles, open circles and the open squares denote experimental values of the averaged moments [7], Fe local moments [41] and the Co local moments [41] respectively. It is clear that our results agree well with the experiments, in particular the qualitative trend of local as well as average magnetic moments. The results show that the Fe local moment increases with increasing Co content up to  $x=0.3$  beyond which it tends towards a saturation while the Co moment remains almost constant for the whole concentration regime. As a result, the average magnetization reaches a maximum at 30% of Co beyond which it starts to decrease. Similar behaviour has been observed in previous studies using LCAO-CPA [39] and LMTO-CPA [42]. This non-monotonic variation of average magnetization can be explained from the variation of local number of electrons (Figure 2) and density of states (Figure 3). In this case, a transition from weak ferromagnetism (incompletely filled majority  $d$  band) for Fe-rich side to strong ferromagnetism (majority  $d$  band completely filled) for alloy with a higher Co content ( $x>0.3$ ) is seen. The initial increase of alloy magnetization corresponds to a continuous filling of majority bands while the minority bands remain almost constantly occupied (Figure 2 (a)). The linear decrease of alloy magnetization with increasing  $x$  for  $x>0.3$  reflects a strong ferromagnetic region in which majority bands are fully occupied whereas the minority bands accommodate more electrons with increasing Co content. The filling of majority band up to  $x=0.3$  mainly occurs due to incompletely filled majority  $d$  band of weak ferromagnet Fe (Figure 2 (b)) while the rise in the minority band filling beyond  $x=0.3$  is essentially due to a fall in

Fe minority electrons and an almost constant nature of Co minority electron number variation (Figure 2 (c)). This is reflected in features of the density of states (Figure 3) as well as variation of the density of states at Fermi level  $n(E_F)$  (Figure 4 (a)). For majority spin states the filling of  $d$  band occurring at Fe sites is accompanied by a steady decrease of  $n(E_F)$ . Upto  $x=0.3$ , the Fermi level is pinned to the minimum of minority spin density of states (Figure 3 (a)- (b)). Increasing Co content, which essentially means gradual filling, shifts the Fermi level to regions of low spin up density of states and above  $x=0.3$  to increasing spin down density of states (Figure 3 (c)-3 (f)). Thus  $n(E_F)$  for up spin (shown by up triangles in Figure 4 (a)) decreases while  $n(E_F)$  for down spin (shown by down triangles) increases continuously beyond  $x=0.3$ . As a result, average  $n(E_F)$  (shown by squares) goes through a minimum around  $x=0.3$ .

All these phenomena are a consequence of local charge neutrality, exchange and hybridization. Since bcc Co is already a saturated ferromagnet, there is hardly any possibility to increase substantially the number of majority spin electrons and thereby the local magnetic moment of Co. Because of small  $sp$ -density of states at Fermi level (Figure 3) compared with the  $d$  contribution, the transfer of minority spin  $d$  electrons to  $sp$ -states is expected to be very small. Thus, Co moment is almost independent of alloy concentration and the possible exchange splitting of Co  $d$  level remains almost constant throughout the concentration regime (Table-1). On the other hand, the weak ferromagnetism of Fe gives rise to the possibility of filling approximately 0.3 majority spin holes with minority spin electrons. Thus, local Fe moment increases as a result of increase in local exchange splitting (Table-1). Hence, inspite of being nearest neighbours in the periodic table the exchange makes their behaviour so very different.

The role of hybridization influencing the local magnetic properties can be explained in terms of the bonding charge transfer (BCT) model [43]. As is evident from the density



| $x_{Co}$ | $\Delta_e^{Fe}$ | $\Delta_e^{Co}$ |
|----------|-----------------|-----------------|
| 0.1      | 0.179           | 0.136           |
| 0.2      | 0.185           | 0.139           |
| 0.3      | 0.190           | 0.140           |
| 0.4      | 0.194           | 0.142           |
| 0.5      | 0.196           | 0.142           |
| 0.6      | 0.199           | 0.142           |
| 0.8      | 0.201           | 0.138           |

**Table 1.** Local exchange splitting values (in Ryd) in  $Co_xFe_{1-x}$  alloys with varying concentration of Co

of states, the disorder in the minority spin band is more prominent which is also realized quantitatively from  $\delta^\sigma$  variation. While  $\delta^\uparrow$  varies from 40 mRyd from Fe-rich side to 6 mRyd in Co-rich side,  $\delta^\downarrow$  remains  $\sim 0.8$  Ryd for the whole range of concentrations. According to the BCT model, different positions of atomic  $d^\downarrow$ -levels of Fe and Co cause bonding charge transfer (BCT) in the minority spin band. An inspection of density of states at various concentrations (Figure 3) shows that the bonding part of spin-up density of states has a larger Co weight whereas Fe dominates the anti-bonding part. A transition of minority spin electrons from Fe to Co occurs. To retain local charge neutrality, mainly Co minority spin electrons are transferred to Fe majority band causing an increase of exchange splitting and magnetic saturation. As a result, a net electron redistribution from  $Fe^\uparrow$  to  $Fe^\downarrow$  state occurs only to increase Fe moment.

So, to conclude, the magnetization behavior of CoFe is characterized on the Fe-rich side by the magnetic saturation due to hybridization whereas the Co-rich side is determined simply by filling of minority band.

Figure 4 (b), 4 (c) and 4 (d) respectively show the variation of inverse susceptibility, spin fluctuation temperature and Curie temperature calculated using MW model. The variation of inverse susceptibility is exactly reverse in nature to that of  $n(E_F)$ . This is due to the fact that inverse susceptibility is dependent on  $n(E_F)^{-1}$  only as stoner

parameter is a constant quantity. The variation of spin fluctuation temperature follows the same nature as of magnetization and inverse susceptibility which are alike and this nature is reflected in Curie temperature because though in the calculations of Curie temperature Stoner Curie temperature was also involved. The diamonds in Figure 4 (d) represent the results of Stoner Curie temperature ( $T_C^S$ ). Apart from much larger values the nature of variation is also non-linear. This is due to the fact that  $T_C^S$  measures the temperature at which the paramagnetic state becomes unstable rather than the magnetic transition temperature.

Figure 5 shows the variation of average and local magnetization in  $\text{Mn}_x\text{Fe}_{1-x}$  alloys with Mn concentration. The filled triangles stand for average value while the filled circles and filled squares represent Fe and Mn local moments respectively. Unfortunately, enough experimental data is not available in this region to support our results. The experimental results so far available (shown by open triangles) [44] agree well with our results. Our results also agree to a reasonable extent with the calculations based on Hartree-Fock-CPA [45] qualitatively but the variation of Mn local moment doesn't agree qualitatively with KKR-CPA results [46]. In our case the Mn local moment linearly decreases with increasing Mn concentration, a feature obtained in Hartree-Fock-CPA calculations too but the KKR-CPA results predict opposite trend for Mn moment. The Fe moment weakly increases and the average moment decreases which is in qualitative agreement with the experimental Slater-Pauling curve [44].

These variations can be explained once again using band filling (Figure 6) and density of states (Figure 7) results. Figure 6 (b) shows an almost constantly filled Fe up and down bands across the concentration regime thereby supporting the weak variation in Fe local moment. In case of Mn, the filling accommodates more number of electrons in the minority band (Figure 6 (c)). As a result, the minority band of the alloy gets

gradually filled up while a loss of electrons from majority bands occur (Figure 6 (a)). This feature is manifested in density of states as well as in variation of  $n(E_F)$  (Figure 8 (a)). For majority spin states the filling of majority band at Fe site reduces  $n(E_F)$  for the corresponding band while increasing Mn content shifts Fermi level to regions of low spin up density of states and high spin down density of states because of gradual filling of minority electrons.

Once again, these phenomena can be explained on the basis of interplay of local charge neutrality, hybridization and magnetic exchange. Unlike Co, Mn  $d$  level exchange splitting varies quite considerably (variation of the order of 30 mRyd) due to gradual filling of the minority band and de-filling of the majority band. As a result, Mn local moment decreases as one goes to Mn rich region. In Fe, since both the bands are nearly filled and a very weak variation of number of local electrons is observed. The local exchange splitting variation is of the order of 14 mRyd only (Table-2). Hence Fe local moment increases, though quite weakly compared to Mn.

| $x_{Mn}$ | $\Delta_e^{Fe}$ | $\Delta_e^{Mn}$ |
|----------|-----------------|-----------------|
| .05      | 0.177           | -0.170          |
| 0.1      | 0.183           | -0.187          |
| .15      | 0.188           | -0.197          |
| 0.2      | 0.191           | -0.202          |

**Table 2.** Local exchange splitting values (in Ryd) in  $Mn_xFe_{1-x}$  alloys with varying concentration of Mn

The role of hybridization and charge re-distribution can be addressed as follows. A look at density of states reveals that unlike FeCo, the disorder is appreciable in both the bands. For the majority band,  $\delta$  increases up to 50 mRyd while  $\delta^\downarrow$  increases around 8 mRyd only. As Mn concentration is increased the bonding part of spin-up density of states is dominated by Fe while the anti-bonding part is dominated by Mn. The reverse situation is observed for spin down density of states. As a result, majority spins

from Mn migrate to Fe and minority spins from Fe migrate to Mn. Thus an increase in Fe local moment is observed. Finally a transition of electrons from  $Mn^\uparrow$  to  $Mn^\downarrow$  state occurs reducing the Mn moment gradually.

Figure 8 (b), (c) and (d) respectively show the results on inverse susceptibility, spin fluctuation temperature and the Curie temperature  $T_C$ . The inverse susceptibility shows a non-linear behaviour and as a result unlike FeCo, we observe a variation of spin fluctuation temperature exactly opposite to that of magnetic moment. But, once again like FeCo,  $T_C$  reflects the behaviour of spin fluctuation temperature though  $T_C^S$  (shown by filled circles in Figure 8 (d)) behaves in a opposite way. These discrepancies are due to limitations of  $T_C^S$  itself which has been discussed for the case of FeCo alloys. Figure 9 shows the concentration dependence of local and average magnetic moments in  $Cr_xFe_{1-x}$  alloy. The solid up triangles represent the calculated average values while the solid circles and solid squares denote the Fe and Cr local moments respectively. Our average magnetization results agree well with the experimental values (shown by open up triangles) [47] and other theoretical results [46, 48, 45]. In fact, for higher Cr concentrations the experimental points almost fall on the theoretical curve establishing good agreement. In case of local moments, our results for Fe agree considerably well with available experimental [48] results but there is quantitative difference in Cr moment values with those of earlier calculations [46, 49]. In our case, we obtain a larger negative value of Cr moment which though increases rapidly in the Cr-rich region but never changes its sign which has been observed in earlier theoretical calculations around  $x=0.7$ . However, this slight discrepancy doesn't affect the average properties at all as is seen from the quantitative agreement with the experiments. Even the qualitative nature of variation of local as well as average moments is well reproduced. As is seen from the figure, Fe moment remains almost constant up to around  $x=0.4$  and then it decreases in

the Cr-rich side but the nature of variation is pretty weak. The Cr moment on the other hand increases rapidly as Cr content is increased making the average value to drop down very fast and approaching zero in accordance with the established observation that the average moment collapses around  $x=0.8$  due to transition from ferromagnetic to antiferromagnetic state.

Once again, we take recourse to the density of states (Figure 11) and variation of local and average number of electrons as number of valence electrons is decreased (Fe-rich to Cr-rich side) (Figure 10) to explain these behaviours. A thorough inspection of density of states for various concentrations show that  $E_F$  is positioned in a valley between the bonding and antibonding peaks in the minority spin density of states. This feature explains the reason for linear variation of average moment because as we keep on increasing Fe content electrons are added to the majority spin states without much affecting minority spins. This feature is very clear in Figure 10 (a). The weak variation of Fe magnetic moment can also be explained likewise. The partial Fe density of states for both spins show little variation across the whole range of concentrations whereas the Cr minority density of states vary appreciably as we scan through the concentration regime. This is understandable if one looks into the variation of majority and minority electrons at each site. In case of Fe (Figure 10 (b)), both the majority and minority bands are almost completely filled while in case of Cr (Figure 10 (c)), the majority band accommodates more and more electrons as Cr-content is increased while the minority band loses and eventually they vary in such a way that at a certain critical concentration there will be more number of electrons in the majority band. Due to this behaviour of Cr, the average number of up electrons decrease (Figure 10 (a)) rapidly in contrast to almost constantly filled minority band in such a way that around  $x=0.8$ , the number of electrons in the majority band will be same as that of minority one establishing a

collapse of magnetic moment when ferromagnetism to antiferromagnetism transition will take place.  $n(E_F)$  variation supports this (Figure 12 (a)). Initially the Fermi level is situated near the  $d$ -level peak in the majority band but as the Cr content is increased and majority band starts losing electrons Fermi level starts moving away from high density of states though initially in the Fe-rich region due to increase in Fe majority band electrons up to  $x=0.4$   $n(E_F)$  had a weak rise. But as we step into Cr-rich region this effect is completely washed out. On the other hand since minority band is almost filled there is almost no variation in  $n(E_F)^\downarrow$ . As a result, the average  $n(E_F)$  has a maxima around  $x=0.4$ .

We now look for investigating the role of hybridization, exchange etc and the type of charge distribution within the constraint of local charge neutrality. In Cr, the local exchange splitting varies more strongly than Mn and also in a opposite way. In case of Mn, exchange splitting decreased towards Mn-rich region whereas in this case, it increases as Cr content is increased (Table-3). The variation in the local exchange splitting for Cr varies of the order of 64 mRyd from a Fe-rich to a Cr-rich region. This is due to the rapid de-filling of Cr minority band. In Fe, since both the bands are nearly filled, the local exchange splitting does not vary as much like that of Cr. Nevertheless, unlike Mn, it decreases and the variation is of the order of 28 mRyd, explaining the decrease of Fe moment.

The charge-redistribution procedure in this case is quite different. Like FeCo, here the disorder in minority bands is stronger as is seen from the  $\delta^\sigma$  values.  $\delta^\downarrow$  varies from 9 mRyd to 2 mRyd from Fe-rich to Cr-rich side while  $\delta^\uparrow$  remains around a value of -0.15 Ryd. This stronger disorder in minority bands indicate a localization of majority electrons. As is seen from the density of states (Figure 11), both the bonding and antibonding part of spin down density of states is dominated by Cr. In case of majority

| $x_{Cr}$ | $\Delta_e^{Fe}$ | $\Delta_e^{Cr}$ |
|----------|-----------------|-----------------|
| .25      | 0.182           | -0.080          |
| 0.4      | 0.179           | -0.059          |
| 0.5      | 0.176           | -0.047          |
| 0.6      | 0.171           | -0.035          |
| 0.7      | 0.163           | -0.024          |
| .75      | 0.158           | -0.020          |
| 0.8      | 0.154           | -0.016          |

**Table 3.** Local exchange splitting values (in Ryd) in  $Cr_xFe_{1-x}$  alloys with varying concentration of Cr

band the bonding part is dominated By Fe and antibonding by Cr. Along with this the nature of variation of number of electrons for both spins at both the constituents (Figure 10) suggest that in this case, unlike the previous two, the electron redistribution occurs mainly between  $Cr^\uparrow$  and  $Cr^\downarrow$  states. Electrons from Cr minority band migrate to Cr majority band explaining the rapid increase of Cr moment.

Figure 12 (b) shows the variation of inverse spin susceptibility of the system with increasing Cr content. Since  $n(E_F)$  has a maxima around  $x=0.4$ , this curve shows a minima around the same region. However, in the case of spin fluctuation temperature variation (Figure 12 (c)) there is no signature of this nature because the effect of magnetic moment variation is much stronger across the concentration region and hence the variation of Spin fluctuation temperature reflects the nature of variation of magnetic moment only. As is seen in the previous two systems, the MW Curie temperature too has a similar nature of variation (shown by solid line in Figure 12 (d)) while  $T_C^S$  values are much higher.

## 5. Conclusions

We have studied the magnetism in bcc based Fe alloys where the three constituents alloyed with Fe belong to the same row of the periodic table and consecutive nearest neighbours of Fe. We have restricted ourselves to the ferromagnetic regions of these alloys only. Our study reveals quite different natures of electronic redistributions among the constituents as we go along from Co to Cr producing different nature of variation of magnetization, Curie temperature and spin susceptibility. We have shown the dominant role of hybridization and magnetic exchange under the constraint of local charge neutrality to explain successfully the variations in magnetic properties of the alloys of nearest neighbours in periodic table.

## Acknowledgements

CBC would like to thank the CSIR, India for financial assistance.

## References

- [1] Ferromagnetic Materials edited by E.P. Wohlfarth and K.H.J. Buschow (North-Holland, Amsterdam, 1980-1993), Vol. 1-7
- [2] Ishikawa Y. in Physics and Applications of INVAR Alloys, *edited* by H. Saito, Honda Memorial Series on Materials Science No. 3 (Moruzen, Tokyo, 1978); Hasegawa H. and Pettifor D.G. 1983 *Phys. Rev. Lett.* **50** 130
- [3] Andersen O.K. *et al* 1977 *Physica B+C* **86-88** 249-256; Kubler J. 1981 *Physics Letters* **81A** 81; Wang C.S., Klein B.M. and Krakauer H. 1985 *Phys. Rev. Lett.* **54** 1852
- [4] Pinski F.J. *et al* 1986 *Phys. Rev. Lett.* **56** 2096; Gonser U., Krische K. and Nasu S. 1980 *Journal of Magnetism and Magnetic Materials* **15-18** 1145; Tsunoda Y. 1988 *J. Phys.: Condens. Matter* **1** 10427; Moruzzi V.L. *et al* 1986 *Phys. Rev.* **B34** 1784
- [5] Hirai K. 1989 *Journal of Phys. Soc. Japan* **58** 4288; Mryasov O.N. *et al* 1991 *J. Phys.: Condens. Matter* **3** 7683; Lichtenstein A.I., Katznelson M.I. and Gubanov V.A. 1984 *J. Phys. F: Met. Phys.* **14** L125; Mryasov O.N., Gubanov V.A. and Lichtenstein A.I. 1992 *Phys. Rev.* **B45** 12330
- [6] Shull C.G. and Wilkinson M.K. 1955 *Phys. Rev.* **97** 304
- [7] Bardos D.I. 1969 *J. Appl. Phys.* **40** 1371
- [8] Collins M.F. and Low G.G. 1965 *Proc. Phys. Soc.* **86** 535
- [9] Child H.R. and Cable J.W. 1976 *Phys. Rev.* **B13** 227



- [10] Radhakrishnan P. and Livet F. 1978 *Solid state comm.* **25** 597
- [11] Kajzar F. and Parette G. 1980 *Phys. Rev.* **B22** 5471
- [12] Arp V., Edmomnds D. and Petersen R. 1952 *Phys. Rev. Lett.* **3** 212, Johnson C.E., Ridout M.S. and Cranshaw T.E. 1963 *Proc. Phys. Soc.* **81** 1079; Lutgemeier H. and Dubiel S.M. 1982 *Journal of Magnetism and Magnetic Materials* **28** 277; Muraoka Y. *et al* 1976 *J. Phys. Soc. Japan* **40** 414; Koi Y., Tsujimura T. and Hihara T. 1964 *J. Phys. Soc. Japan* **19** 1493
- [13] Stoelinga J.H.M. and Gersdorf R. 1966 *Physics Letters* **19** 640
- [14] Cheng C.H., Wei C.T. and Beck P.A. 1960 *Phys. Rev.* **2** 426
- [15] Scroder K. 1962 *Phys. Rev.* **125** 1209
- [16] Van Baal C.M. 1973 *Physica* **64** 571; Kikuchi R. and Sato H. 1974 *Acta Metall.* **22** 1099; Umabayashi H. and Ishikawa Y. 1966 *J. Phys. Soc. Japan* **21** 1281
- [17] Hasegawa H. and Kanamori J. 1972 *J. Phys. Soc. Japan* **33** 1607; Matthews J.C. 1972 *J. Phys. Soc. Japan* **32** 110
- [18] Jo T. 1982 *J. Phys. Soc. Japan* **3** 794
- [19] James P. *et al* 1999 *Phys. Rev.* **B59** 419; Schwarz K. *et al* 1984 *J. Phys. F: Met. Phys.* **14** 2659
- [20] Burke S.K. and Rainford B.D. 1983 *J. Phys. F: Met. Phys.* **13** 441; Ebert H. *et al* 1990 *J. Phys.: Condens. Matter* **2** 443; Martinez-Herrera F.J. *et al* 1985 *Phys. Rev.* **B31** 1686; Drittler B. 1989 *et al Phys. Rev.* **B40** 8203
- [21] Akai H. and Dederichs P.H. 1993 *Phys. Rev.* **B47** 8739; Bluegel S. *et al* 1987 *Phys. Rev.* **B35** 3271; Turek I. *et al* 1994 *Phys. Rev.* **B49** 3352
- [22] Paduani C. and Krause J.C. 1998 *Phys. Rev.* **B58** 175; Dederichs P.H. *et al* 1991 *Journal of Magnetism and Magnetic Materials* **100** 241; Kaspar J. and Salahub D.R. 1983 *J. Phys. F: Met. Phys.* **13** 311; Qiu S.L., Marcus P.M. and Moruzzi V.L. 1998 *Phys. Rev.* **B58** 2651
- [23] Kulikov N.I. and Tugushev V.V. 1984 *Sov. Phys. Usp* **27** 954; Fawcett E. *et al* 1994 *Rev. Mod. Phys.* **66** 25; Furuska M. *et al* 1986 *J. Phys. Soc. Japan* **55** 2253
- [24] Endoh Y. and Ishikawa Y. 1971 *J. Phys. Soc. Japan* **30** 1614
- [25] Mookerjee A. and Prasad R. 1993 *Phys. Rev.* **B48** 17724
- [26] Saha T., Dasgupta I. and Mookerjee A. 1994 *Phys. Rev.* **B50** 13267
- [27] Sanyal B. *et al* 1998 *J. Phys.: Condens. Matter* **10** 5767
- [28] Andersen O K, Jepsen O and Glotzel 1985 *Highlights of Condensed-Matter Theory*, edited by Bassani F, Fumi F and Tosi M P (North-Holland, New York), p. 59
- [29] Biswas P.P. *et al* 1995 *J. Phys.: Condens. Matter* **7** 8569
- [30] Luchini M U and Nex C M M 1987 *J. Phys. C: Solid State Phys.* **20** 3125
- [31] Ghosh S, Das N and Mookerjee A 1997 *J. Phys.: Condens. Matter* **9** 1701
- [32] Mohn P H and Wolfarth E P 1987 *J. Phys. F* **17** 2421
- [33] Janak J.F. 1977 *Phys. Rev.* **B16** 255
- [34] Gunnarson O 1976 *J. Phys. F* **6** 587
- [35] Gersdorf R 1962 *J. Phys. Radium* **23** 726
- [36] Saha T, Dasgupta I and Mookerjee A 1996 *J. Phys.: Condens. Matter* **8** 1979
- [37] Ghosh S., Das N. and Mookerjee A. 1999 *Modern Phys. Letters* **B13** 723
- [38] Turek I. *et al* in *Electronic structure of disordered alloys, surfaces and interfaces* 1997, Kluwer Academic Publishers
- [39] Richter R. and Eschrig H. 1988 *J. Phys. F: Met. Phys.* **18** 1813
- [40] Schwarz K. and Salahub D.R. 1982 *Phys. Rev.* **B25** 3427

- [41] Collins M.F. and Forsyth J.B. 1963 *Phil. Mag.* **8** 401
- [42] Turek I. *et al* 1994 *Phys. Rev.* **B49** 3352
- [43] Richter R. and Eschrig H. 1987 *Proc. 7th General EPS conf.*, Pisa
- [44] Fisher H. *et al* in *Magnetic Ultrathin Films, Multilayers and Surfaces*, edited by A. Fert *et al*, MRS symposia proceedings No. 384 (Materials Research Society, Pittsburgh, 1995)
- [45] Hasegawa H. and Kanamori J. 1972 *J. Phys. Soc. Japan* **33** 1607
- [46] Kulikov N.I. and Demangeat C. 1997 *Phys. Rev.* **B55** 3533
- [47] Ling M.F., Staunton J.B. and Johnson D.D. 1995 *J. Phys. C: Solid State Phys.* **7** 1863
- [48] Buttler W.H. *et al* 1995 *Journal of Magnetism and Magnetic Materials* **151** 354
- [49] Dederichs P.H. *et al* 1991 *Journal of Magnetism and Magnetic Materials* **100** 241

## Figure Captions

**Figure 1** Partial and averaged magnetic moments (in Bohr-magneton/atom) vs. concentration of Co for  $\text{Co}_x\text{Fe}_{1-x}$  alloy. The solid line with filled up triangles represents calculated averaged values, the solid line with filled circles represents calculated Fe moments, the solid line with filled squares represents calculated Co moments. The open up triangles are the experimental values of average moments, the open circles are the experimental Fe moments and the open squares are the experimental Co moments.

**Figure 2** (a) represents average number of valence electrons for both spins vs. concentration of Co for  $\text{Co}_x\text{Fe}_{1-x}$  alloy. (b) represents number of electrons at Fe site for both spins vs. concentration of Co. (c) represents number of electrons at Co site for both spins. The up and the down triangles are for the spin-up and for the spin-down electrons respectively for all the three cases.

**Figure 3** Spin projected partial and averaged densities of states of  $\text{Co}_x\text{Fe}_{1-x}$  alloy. The various panels are for different concentrations of Co- (a)10% (b)20% (c)40% (d)50% (e)60% (f)80%. In all the cases, the solid line represents averaged density of states while the dashed and the dotted line stand for Co and Fe partial density of states respectively.

**Figure 4** (a) represents density of states at Fermi level for both spins as well as the averaged values vs. concentration of Co in  $\text{Co}_x\text{Fe}_{1-x}$  alloy. The up and down triangles stand for values of up and down spins respectively while the squares stand for averaged values. (b) represents averaged inverse spin susceptibilities ( $2\mu_B^2/\chi$  in Ryd-atom vs. concentration of Co in  $\text{Co}_x\text{Fe}_{1-x}$  alloy. The circles represent the calculated values. (c) represents variation of spin fluctuation temperature ( $T_{SF}$ ) in

Kelvin vs. concentration of Co in  $\text{Co}_x\text{Fe}_{1-x}$  alloy. (d) the solid line and the filled circles represent the variation of Curie temperature ( $T_C$ ) in Kelvin calculated using MW model vs Co concentration. The diamonds stand for the values of Stoner Curie temperature ( $T_C^S$ ) in Kelvin.

**Figure 5** Partial and averaged magnetic moments (in Bohr-magneton/atom) vs. concentration of Mn for  $\text{Mn}_x\text{Fe}_{1-x}$  alloy. The solid line with up triangles represents calculated averaged values, the solid line with filled circles represents calculated Fe local moments, the solid line with filled squares represents calculated Mn local moments. The open up triangles are for the experimental values of the average moments.

**Figure 6** (a) represents average number of valence electrons for both spins vs. concentration of Mn for  $\text{Mn}_x\text{Fe}_{1-x}$  alloy. (b) represents number of electrons at Fe site for both spins vs. concentration of Mn. (c) represents number of electrons at Mn site for both spins. The up and the down triangles are for the spin-up and for the spin-down electrons respectively for all the three cases.

**Figure 7** Spin projected partial and averaged densities of states of  $\text{Mn}_x\text{Fe}_{1-x}$  alloy. The various panels are for different concentrations of Mn- (a)5% (b)10% (c)15% (d)20% . In all the cases, the solid line represents averaged density of states while the dashed and the dotted line stand for Mn and Fe partial density of states respectively.

**Figure 8** (a) represents density of states at Fermi level for both spins as well as the averaged values vs. concentration of Mn in  $\text{Mn}_x\text{Fe}_{1-x}$  alloy. The up and down triangles stand for values of up and down spins respectively while the squares stand for averaged values. (b) represents averaged inverse spin susceptibilities ( $2\mu_B^2/\chi$  in Ryd-atom vs. concentration of Mn in  $\text{Mn}_x\text{Fe}_{1-x}$  alloy. The circles represent the

calculated values. (c) represents variation of spin fluctuation temperature ( $T_{SF}$ ) in kelvin vs concentration of Mn in  $Mn_xFe_{1-x}$  (d) the solid line and the filled circles represent the variation of Curie temperature ( $T_C$ ) in Kelvin calculated using MW model vs. Mn concentration. The diamonds stand for the values of Stoner Curie temperature ( $T_C^S$ ) in Kelvin.

**Figure 9** Partial and averaged magnetic moments (in Bohr-magnetons/atom) vs. concentration of Cr for  $Cr_xFe_{1-x}$  alloy. The solid line with up triangles represents calculated averaged values, the solid line with filled circles represents calculated Fe local moments, the solid line with filled squares represents calculated Cr local moments. The open up triangles are for the experimental values of average moments and the open circles are for the experimental Fe moments.

**Figure 10** (a) represents average number of valence electrons for both spins vs. concentration of Cr for  $Cr_xFe_{1-x}$  alloy. (b) represents number of electrons at Fe site for both spins vs. concentration of Cr. (c) represents number of electrons at Cr site for both spins. The up and the down triangles are for the spin-up and for the spin-down electrons respectively for all the three cases.

**Figure 11** Spin projected partial and averaged densities of states of  $Cr_xFe_{1-x}$  alloy. The various panels are for different concentrations of Cr- (a)25% (b)40% (c)50% (d)60% (e)70% (f)80%. In all the cases, the solid line represents averaged density of states while the dashed and the dotted line stand for Cr and Fe partial density of states respectively.

**Figure 12** (a) represents density of states at Fermi level for both spins as well as the averaged values vs. concentration of Cr in  $Cr_xFe_{1-x}$  alloy. The up and down triangles stand for values of up and down spins respectively while the squares stand

for averaged values. (b) represents averaged inverse spin susceptibilities ( $2\mu_B^2/\chi$ ) in Ryd-atom vs. concentration of Cr in  $\text{Cr}_x\text{Fe}_{1-x}$  alloy. The circles represent the calculated values. (c) represents variation of spin fluctuation temperature ( $T_{SF}$ ) in Kelvin vs. concentration of Cr in  $\text{Cr}_x\text{Fe}_{1-x}$  (d) the solid line and the filled circles represent the variation of Curie temperature ( $T_C$ ) in Kelvin calculated using MW model vs Cr concentration. The diamonds stand for the values of Stoner Curie temperature ( $T_C^S$ ) in Kelvin.

Figure 1

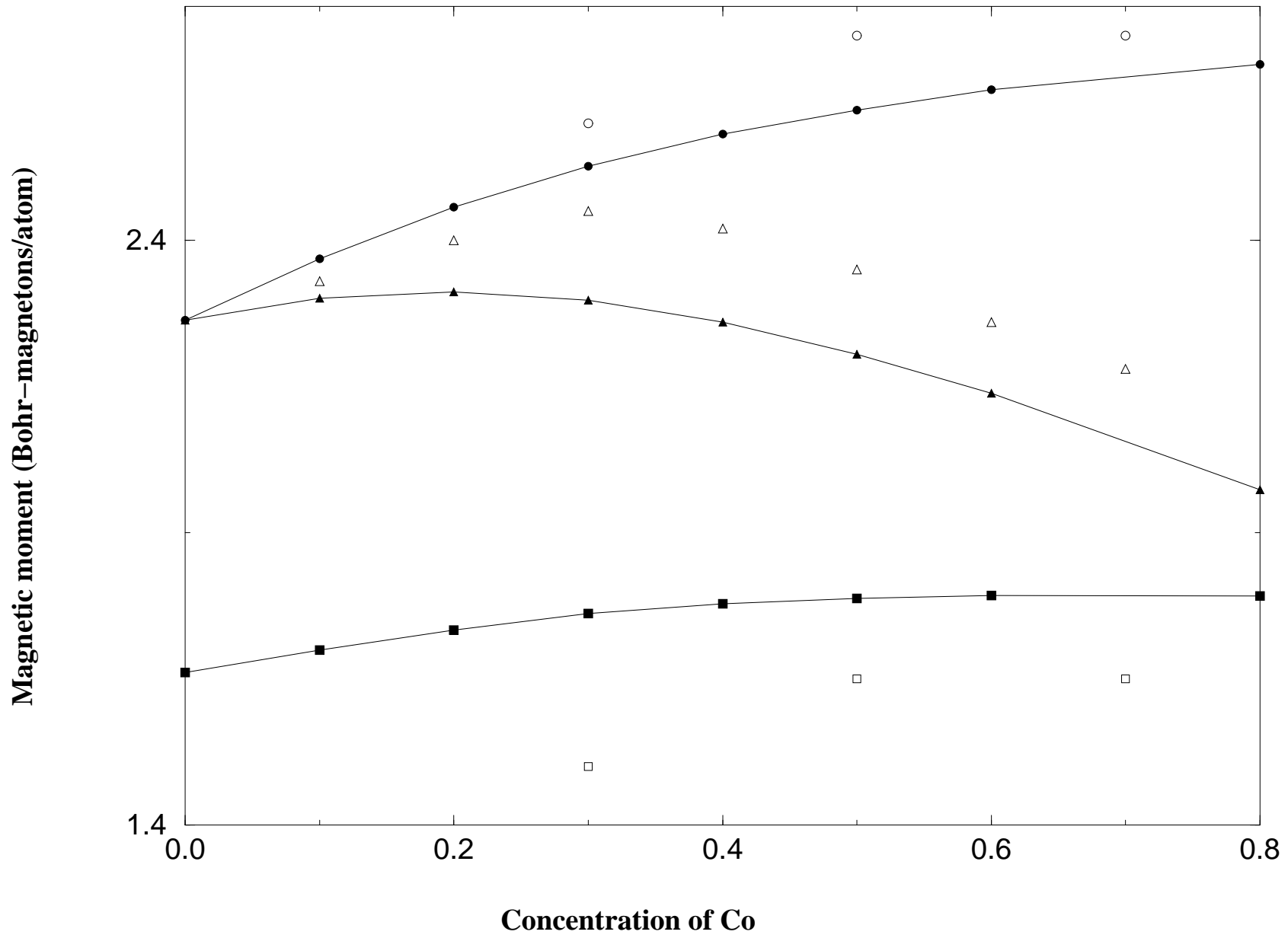
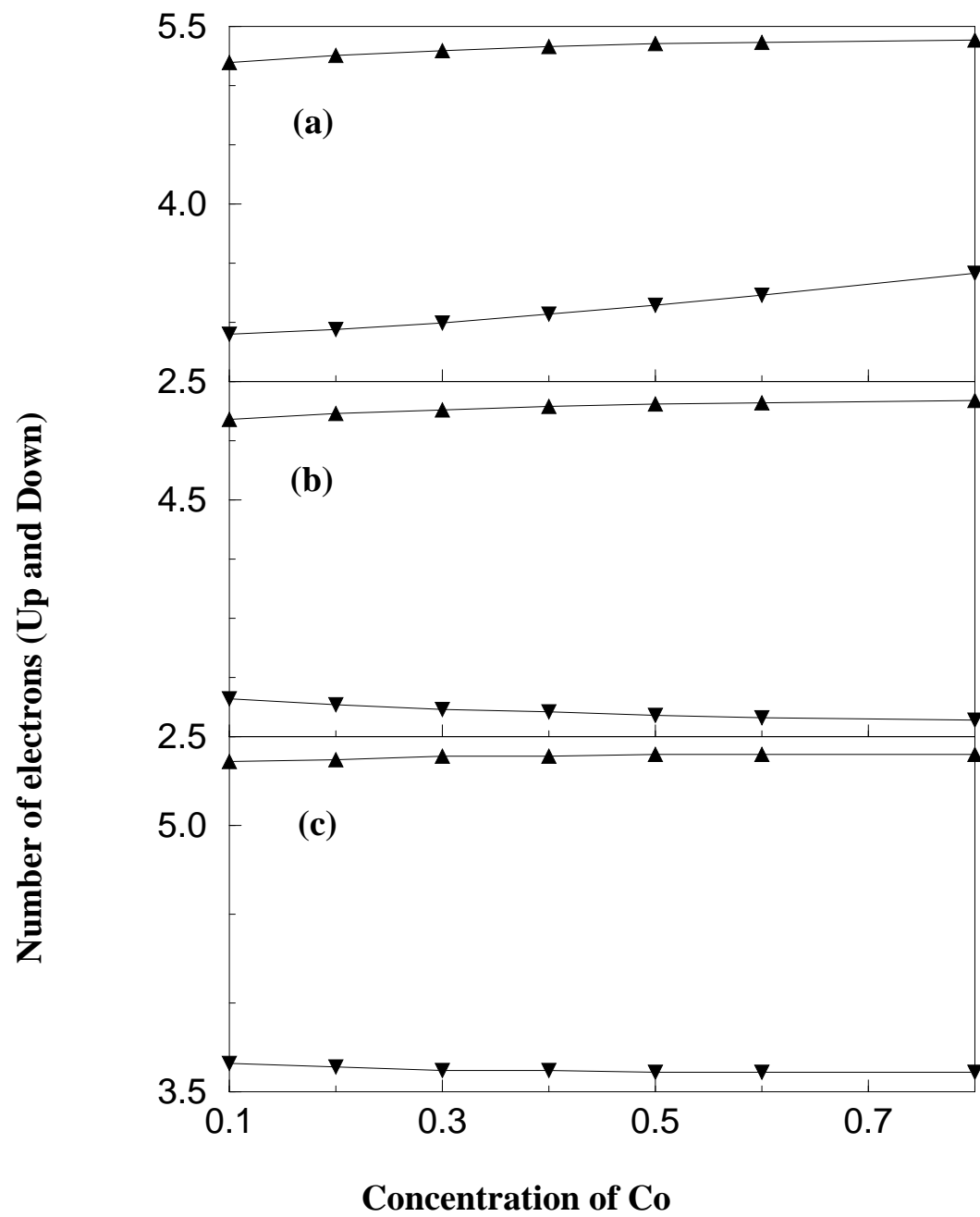
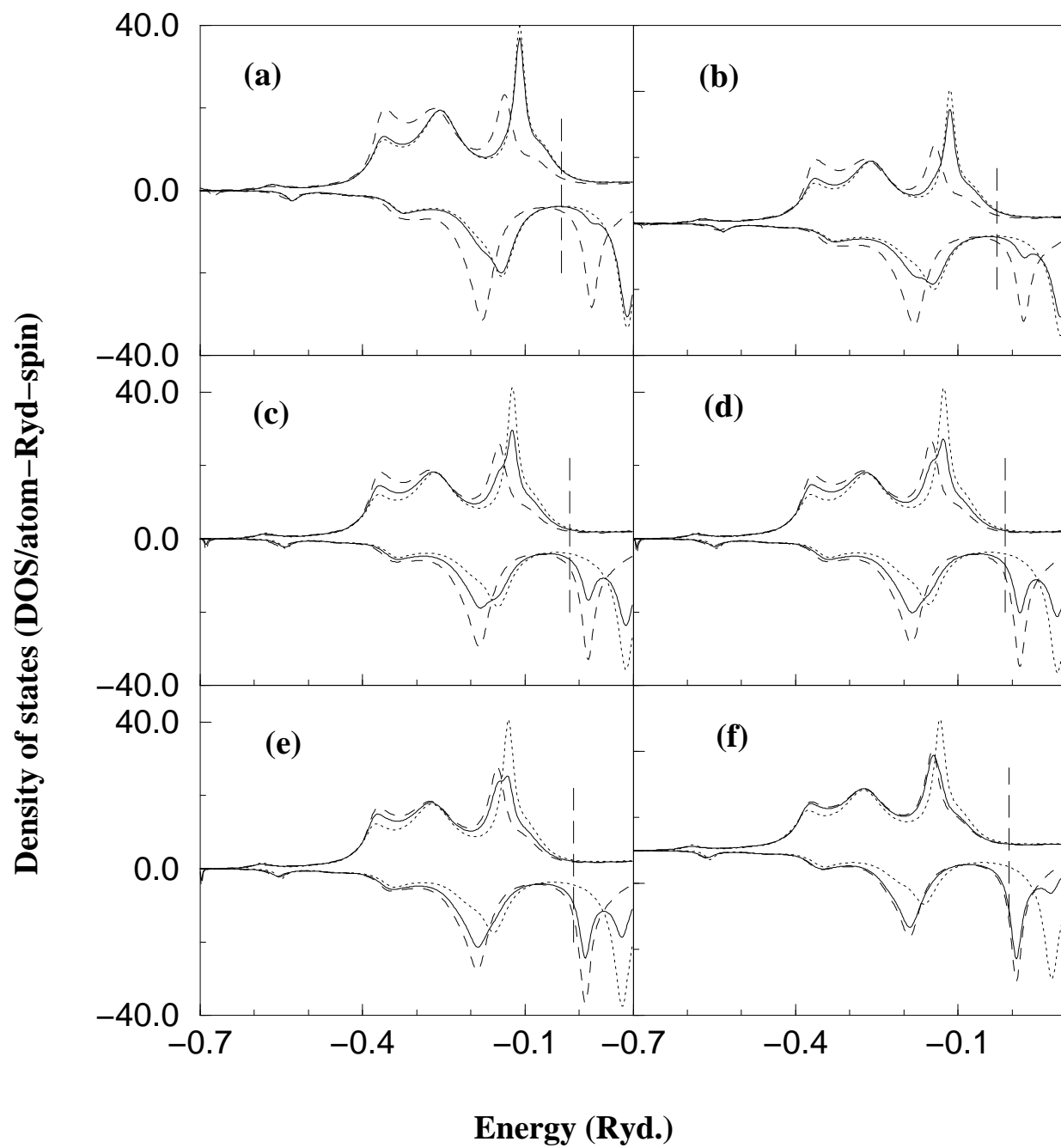


Figure 2

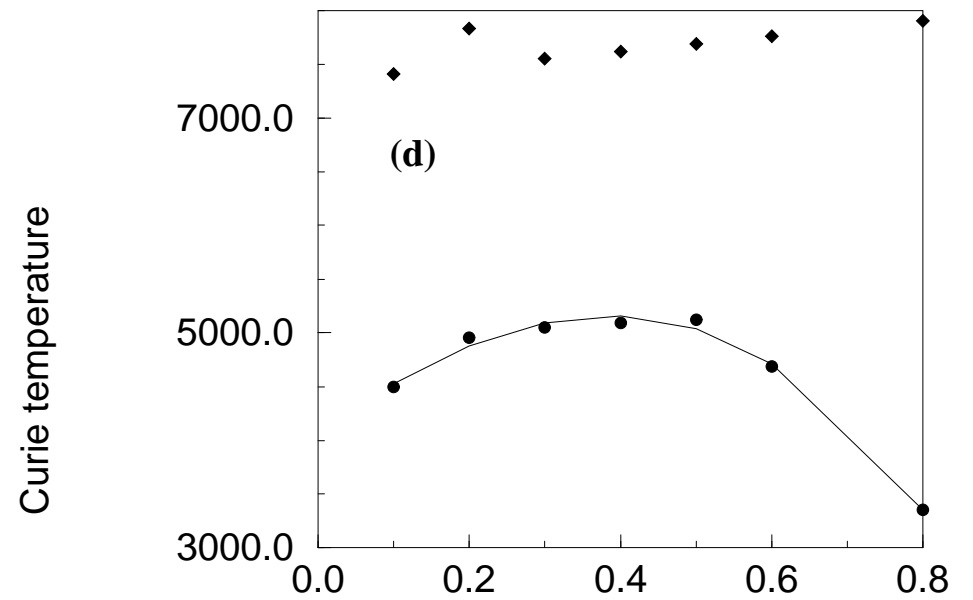
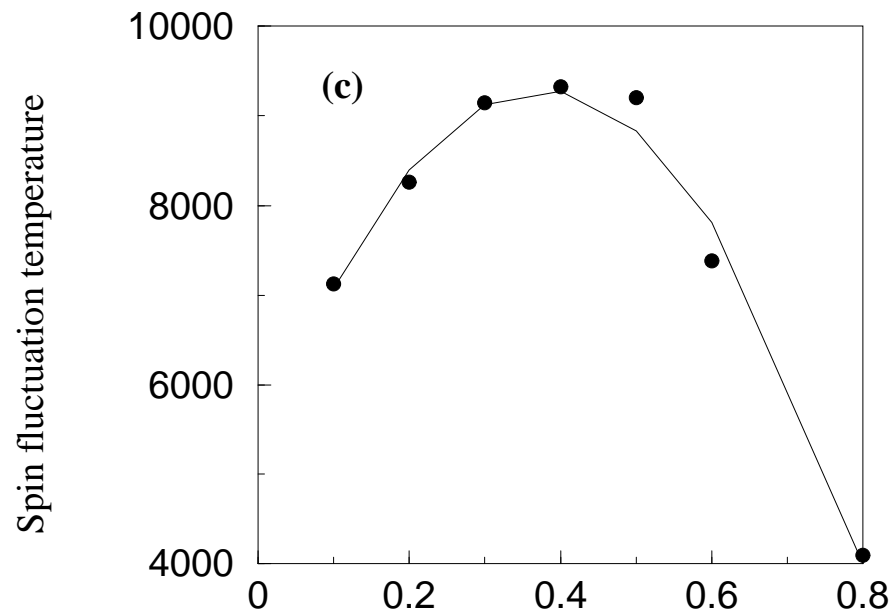
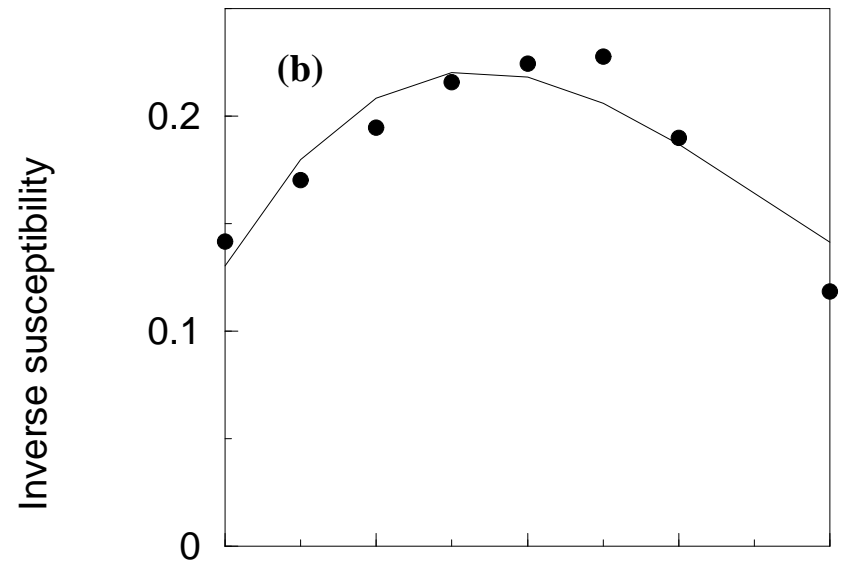
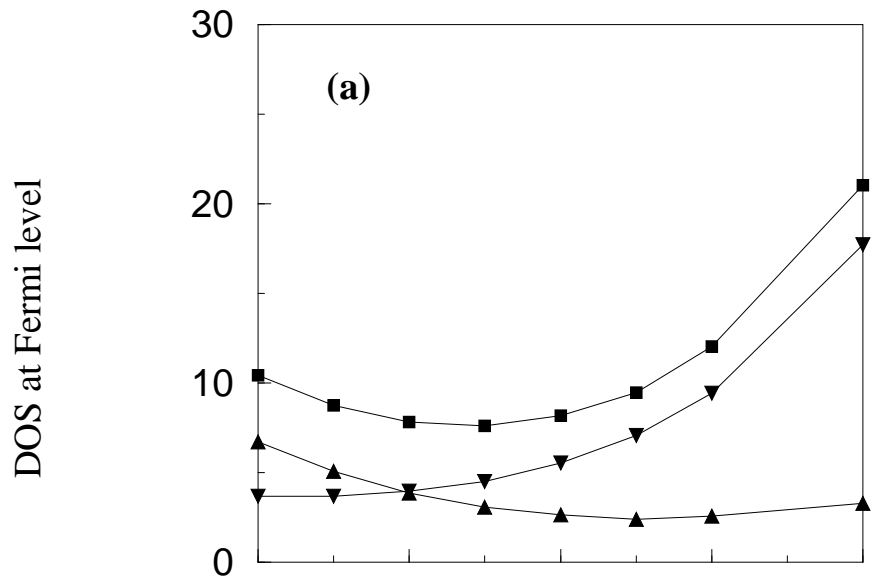




**Figure 3**



**Figure 4**



**Concentration of Co**

Figure 5

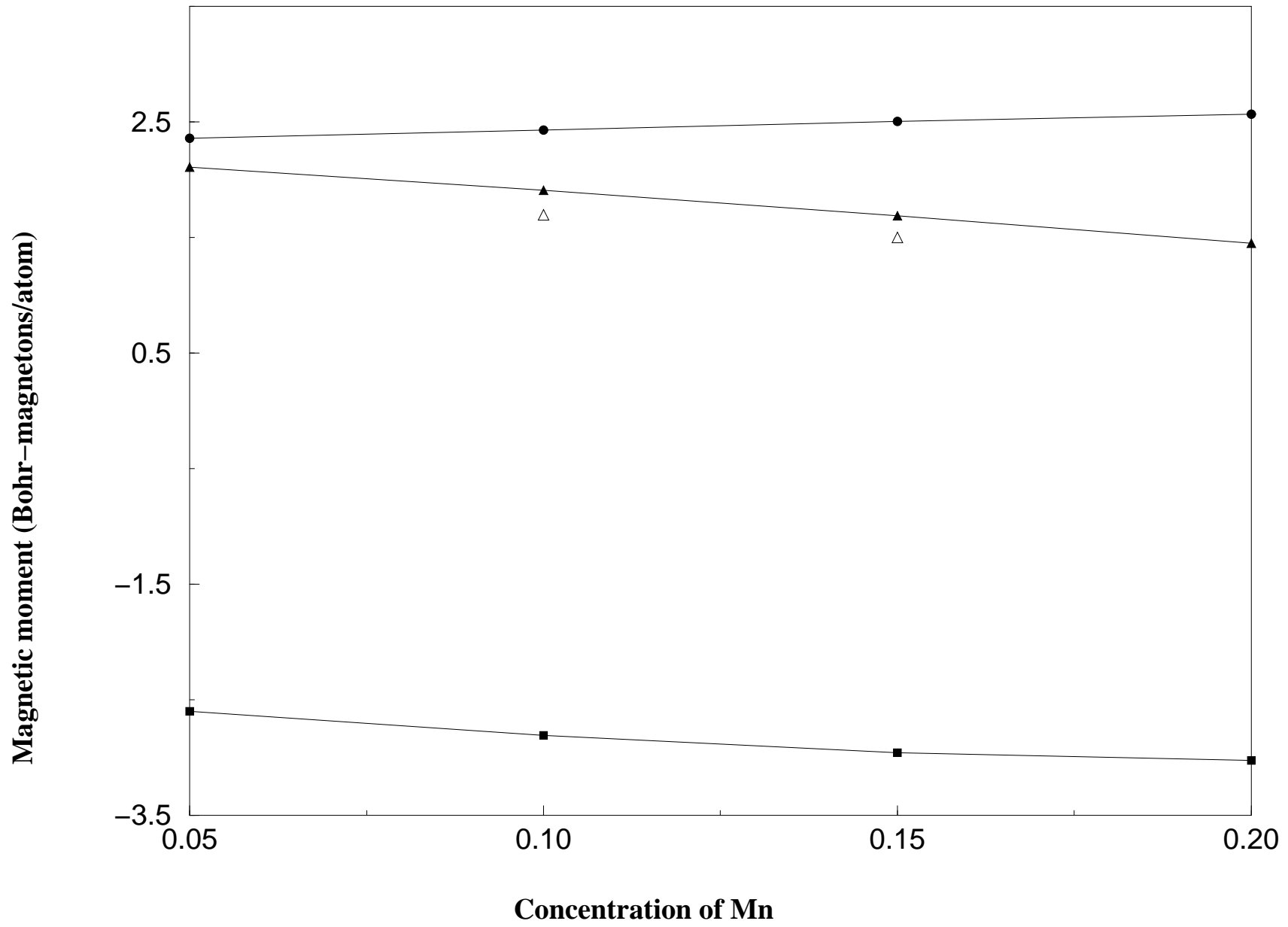


**Figure 6**

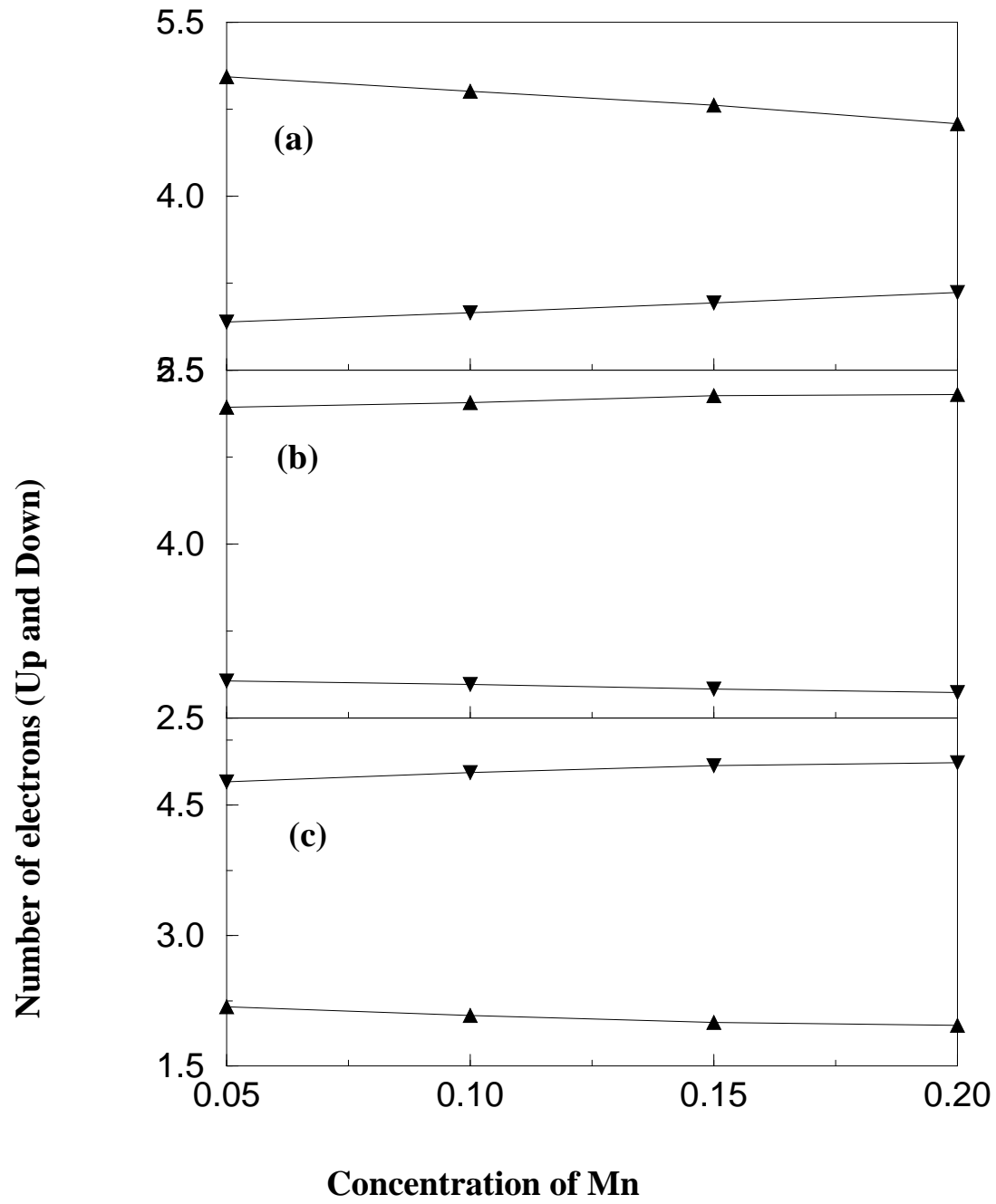


**Figure 7**

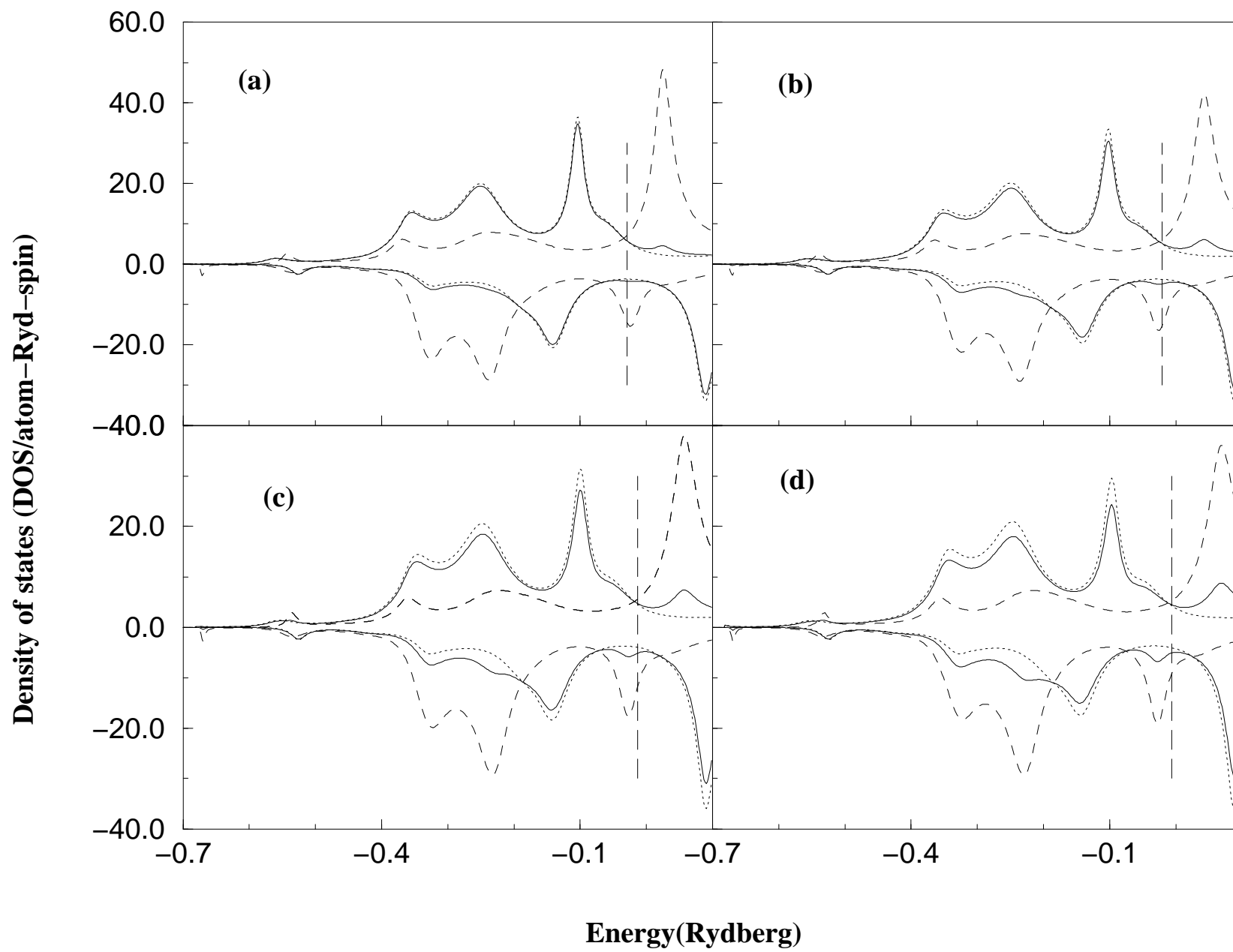


**Figure 8**

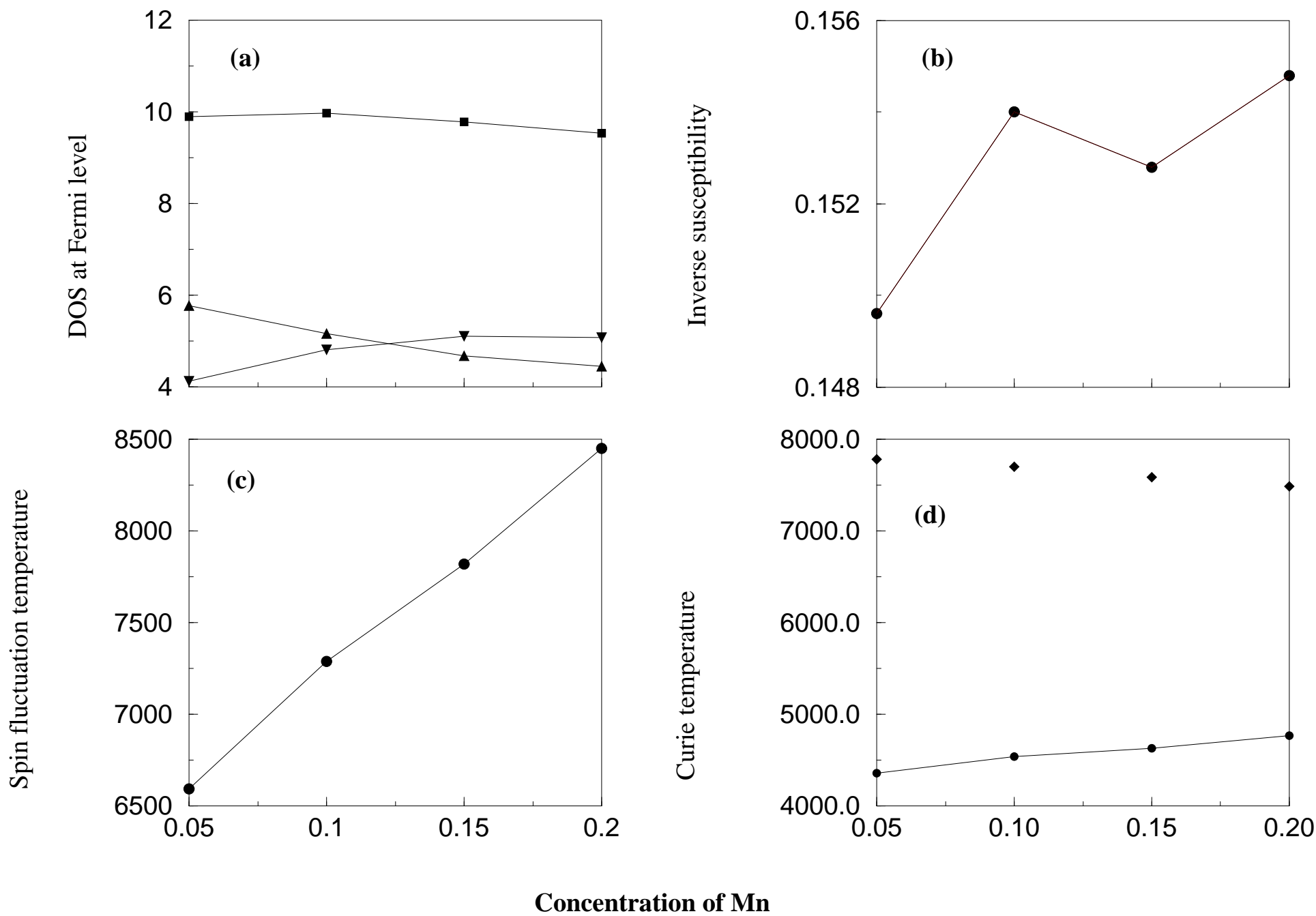


Figure 9

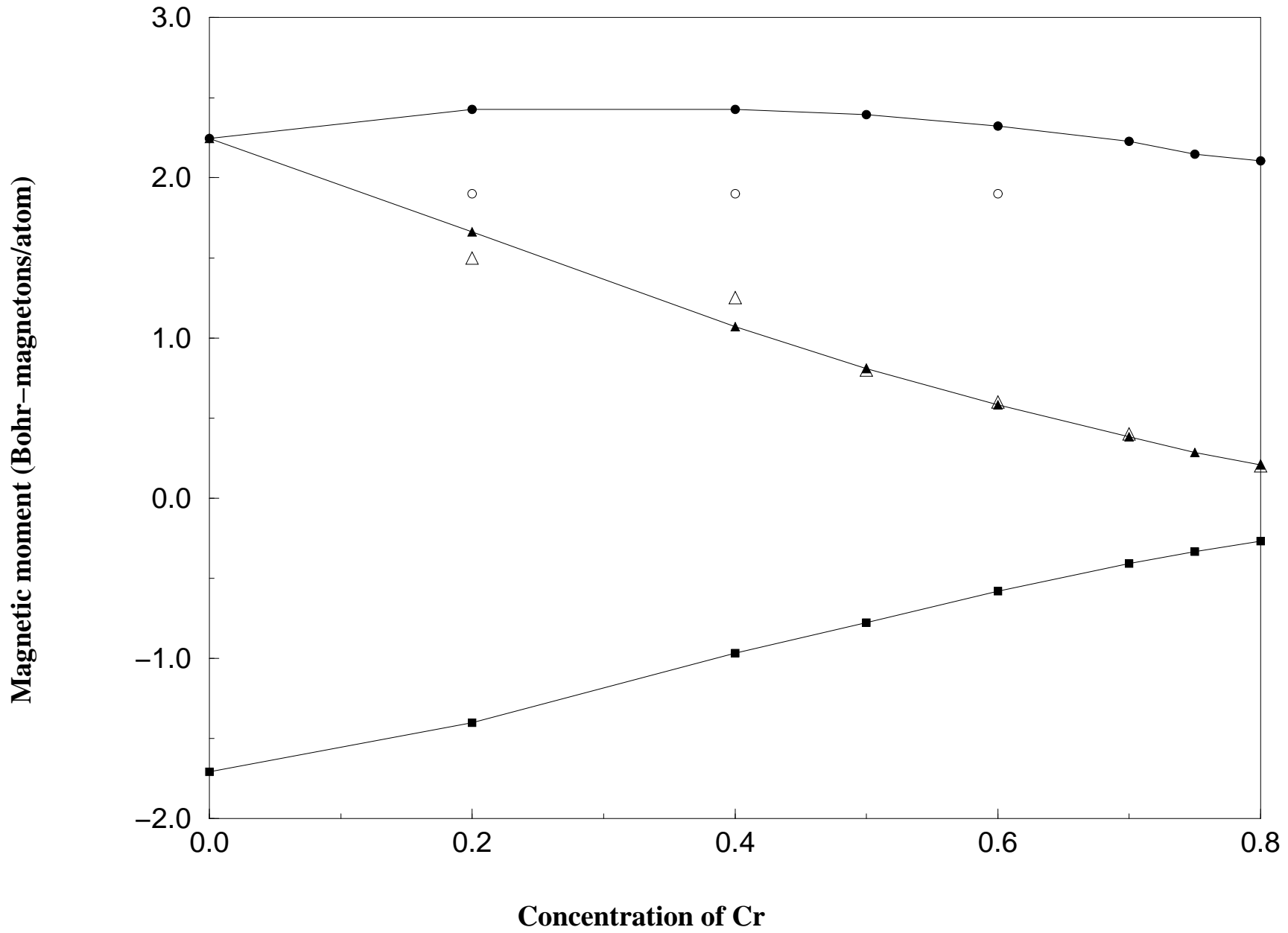
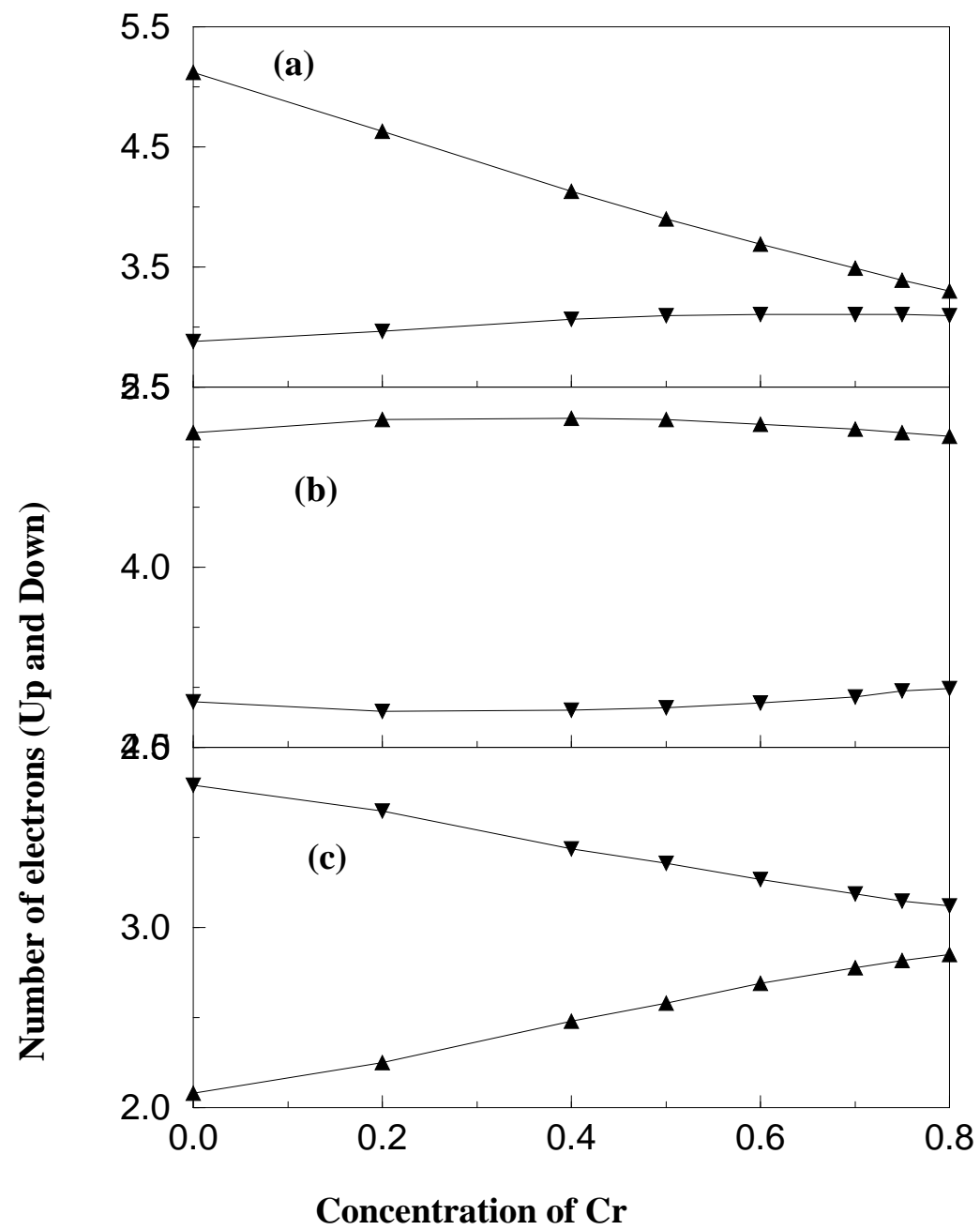


Figure 10





**Figure 11**

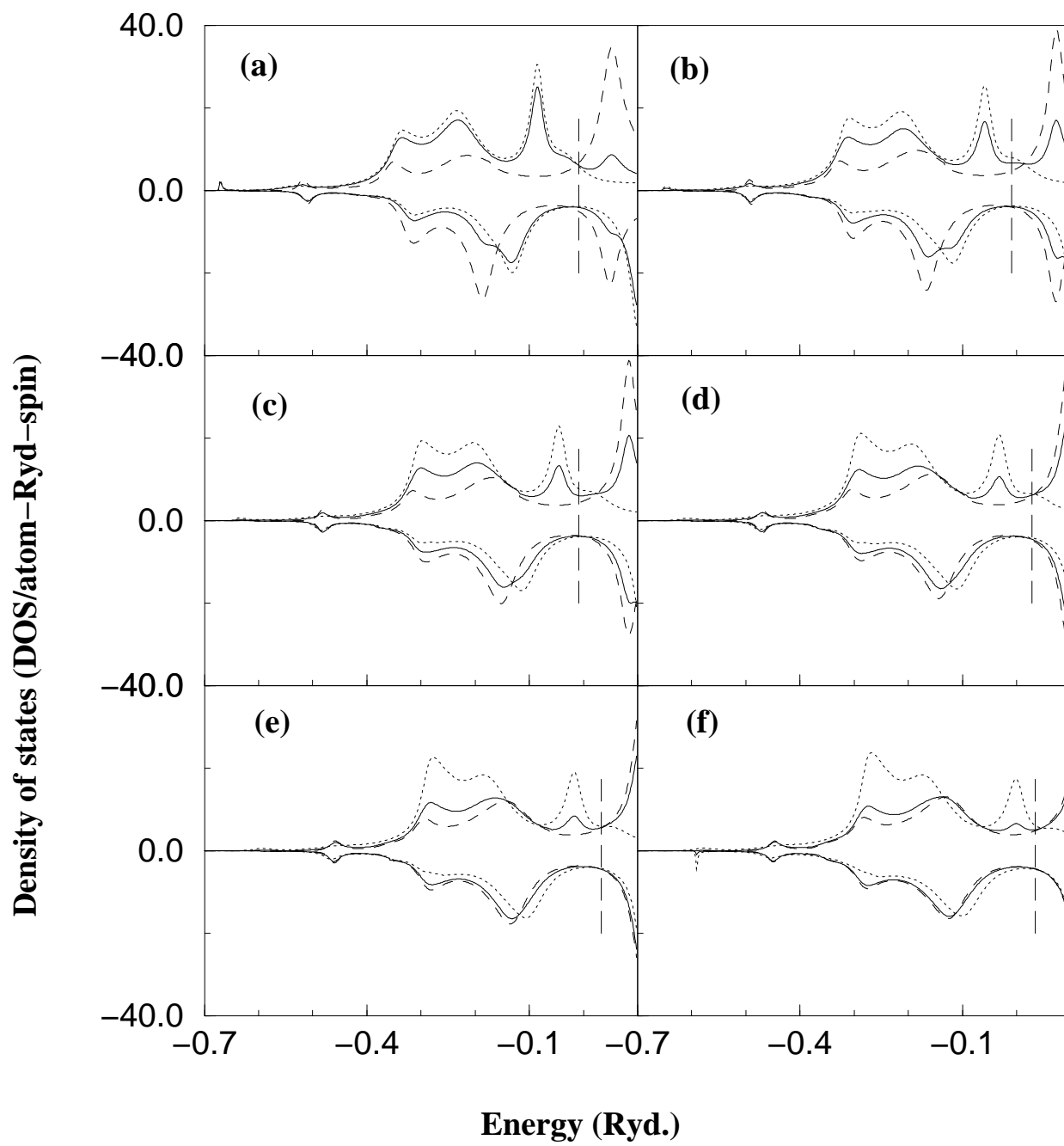


Figure 12

